Morphology and Barrier Properties of Nanobiocomposites of Poly(3-hydroxybutyrate) and Layered Silicates

M. D. Sanchez-Garcia,[1] E. Gimenez,[2] J. M. Lagaron[1]

[1]*Novel Materials and Nanotechnology, IATA, CSIC, Apdo Correos 73, Burjassot 46100, Spain*
[2]*Area of Materials, Department of Industrial Systems Engineering and Design, University Jaume I, Castelló 12071, Spain*

Received 28 May 2007; accepted 2 October 2007
DOI 10.1002/app.27622
Published online 25 February 2008 in Wiley InterScience (www.interscience.wiley.com).

ABSTRACT: Polyhydroxybutyrate (PHB) is generally considered to be a very uneasy biopolymer to handle because of significant instability during melt processing and some excessive brittleness. This work studied the morphological, thermal, and barrier properties of novel melt-mixed nanobiocomposites of PHB, poly(ε-caprolactones) (PCL), and layered phyllosilicates based on commercial organomodified kaolinite and montmorillonite clay additives. The addition of PCL component to the blend was seen to reduce oxygen permeability but it was also found to lead to a finer dispersion of the clay. The addition of highly intergallery swollen organomodified montmorillonite clays to the PHB blend led to a highly dispersed morphology of the filler, but this simultaneously increased to a significant extend the melt instability of the biopolymer. Nevertheless, the organomodified kaolinite clay, despite the fact that it was found to both lead to less dispersed and irregular morphology, particularly for higher clay loadings, it led to enhanced barrier properties to oxygen, D-limonene, and water. D-limonene and specially water molecules were, however, found to sorb in both hydrophobic and hydrophilic sites of the filler, respectively, hence diminishing the positive barrier effect of an enlarged tortuosity factor in the permeability. Mass transport properties were found to depend on the type of penetrant and modeling of the permeability data to most commonly applied formalisms was not found to be satisfactory because of factors such as morphological alterations, heterogeneity in the clay dispersion, and penetrant solubility in the filler.
 J Appl Polym Sci 108: 2787–2801, 2008

Key words: biopolymers; packaging applications; barrier properties; nanocomposites; polyhydroxybutyrate

INTRODUCTION

In the last decades, there has been a significant increase in the amount of plastics being used in packaging applications. In fact, the largest application for plastics today is packaging, and within the packaging niche, food packaging amounts has the largest plastics demanding application. This substantial increase in use has also raised a number of environmental concerns from a waste management point of view.[1–3] As a result, there is a strong research interest, pushed by authorities at national and international levels, and a parallel industrial growing demand in the development and use of materials which can disintegrate and biodegrade through processes such as composting into carbon dioxide and water.

Among biodegradable materials, three families[1–4] are usually considered: polymers directly extracted from biomass such as the polysaccharides starch, chitosan, and cellulose and proteins such as gluten, soy protein, and zein. A second family comprises oil based monomers or biomass derived monomers, but uses classical chemical synthetic routes to obtain the final biodegradable material, this is the case of for instance poly(ε-caprolactones) (PCL), polyvinyl-alcohol (PVOH) and for the case of sustainable monomers polylactic acid (PLA). The third family comprises polymers produced by natural or genetically modified microorganisms such as polyhydroxylalcanoates and polypeptides.[5]

Recently, surface modified clays have been studied as advanced additives to improve or balance thermal, mechanical, fire resistance, surface, or conductivity properties of nanocomposites because of its high surface to volume ratios and the subsequent intimate contact that they promote with the matrix at low filler additions.[5] Aside from the enhancement in these properties, these clay platelets with very few nanometers (ideally one nanometer in fully exfoliated systems) in thickness have the potential to uniquely reduce the matrix permeability to gases and vapors,

Correspondence to: J. M. Lagaron (lagaron@iata.csic.es).
Contract grant sponsor: EU integrated project SUSTAINPACK.
Contract grant sponsor: CYCIT project; contract grant numbers: MAT2006-10261-C03-01, MAT2003-08480-C3.

while maintaining largely unmodified interesting properties of the matrix such as toughness or transparency. The enhanced gas barrier properties of polymer nanocomposites are now finding some specific applications, in fields such as membranes and in packaging materials and containers for a wide variety of food and beverage products.[6,7]

Kaolinite ($Al_2Si_2O_5(OH)_4$) is a naturally occurring 1 : 1 phyllosilicate containing a gibbsite (aluminum hydroxide) octahedral layer and a silicon oxide tetrahedral sheet. This asymmetric structure allows the formation of hydrogen bonds between consecutive layers, providing a large cohesive energy. As a consequence of the high layer-to-layer interactions, the intercalation of the polymer chains in between the kaolinite platelets is greatly impeded, being thus a necessary layer for surface chemical treatment to facilitate the intercalation and further exfoliation of the clay. The treatment usually consists of an intercalation of chemical agents such as poly(ethylene glycol), *n*-methyl formamide, 1-methyl-2-pyrrolidone, 6-aminohexanoic acid, methanol, octadecylamine, or even polyhydroxybutyrate (PHB) (Ref. 8 and therein). Montmorillonite, unlike kaolinite, is strongly prone to swelling with increasing water content and is, therefore, a highly hydratable naturally occurring 2 : 1 phyllosilicate consisting of a central gibbsite octahedral layer between two external silica tetrahedral sheets. Isomorphous substitution of the Al^{3+} within the layers by for instance Fe^{2+} or Mg^{2+} yields a positive charge deficiency (characterized by the so-called cation exchange capacity), which is balanced by hydrated cations (Na^{1+}, Li^{1+}, Ca^{2+}) at the interlayer.[9] Water molecules are, therefore, more strongly present in montmorillonite clays. Blends of thermoplastic biodegradable polymers, such PCL, PLA, and PHB, and the pure clay materials are typically incompatible; as a result, incorporation of an organic modifier onto the clay surface, to mediate between the polarity of the hydrophilic clay surface and that of the more hydrophobic polymer, has been widely adopted for compatibilization and for ease of exfoliation of the clay platelets into the polymer matrix during processing. Thus, as expected, the organoclay dispersability within a polymer matrix has been found to depend on factors such as type and quantity of surfactant, type of clay employed, as well as on the processing conditions. In the latter respect, the most interesting method for preparing polymer-based nanocomposites is the melt compounding route. This route is most adequate for rapid industrial implementation of the technology because of the wide availability of melt processable equipment and applications.[9–12]

Biodegradable thermoplastic polyesters are melt processable biomaterials that present a number of excellent and promising properties in a number of uses, including packaging, automotive, and biomedical applications. Among them, bacterial biopolymers such as poly(3-hydroxybutyrate) (PHB) and its copolymers with valerate (PHB/HV) present good thermal, permselectivity, and mechanical properties. However, PHB suffers from relatively medium to low barrier to gases and water vapor, lack of transparency, brittleness and, more importantly, low melt stability.[13,14] A feasible strategy to decrease the inherent brittleness of thermoplastic biopolymers is by blending with PCL.[4,15–18] PCL is also a biodegradable polyester obtained by ring-opening polymerization from the ε-caprolactone. The PCL is a semicrystalline polymer with low tensile strength, high elongation at break (above 400%), and processing temperatures similar to biopolyesters, therefore, it is expected to act as a plasticizing agent when blending it with for instance the PLA and PHB polymers. A potential drawback of these materials is the increase in gas permeability exhibited by the blends because of the poorer gas barrier properties of PCL. Nanocomposites of PCL have already been found to decrease by up to 50% the oxygen permeability of the polymer and to exhibit enhanced thermal and mechanical stability.[19] Previous work in our group in nanobiocomposite blends of an amorphous poly(lactic acid), PCL, and a food contact complying modified kaolinite were found to lead to a unique balance of thermal, mechanical, and barrier properties.[20,21]

Solvent casting nanocomposites of PHB with organically modified montmorillonite having as surfactants organic quaternary ammonium salts have previously been reported.[22] These solution cast composites displayed intercalated morphologies and exhibited improved thermal stability, except for contents of clay in excess of 6%. Not many blending works have, however, been carried out with PHB by direct melt compounding because of its melt instability.[13,14] However, a recent study showed that melt blending of PHB with various plasticizers has been proven to be a feasible route to enhance the biopolymer melt stability as determined by DSC.[13] Nanocomposites via melt compounding have only been developed for PHB/HV copolymers.[23] The results showed that good dispersion of the fillers and enhanced temperature and rate of crystallization were achieved. PHB/HV copolymers have lower melting temperature and, therefore, can overcome the low melt stability of the neat PHB, but have as drawback low crystallization kinetics and lower barrier properties. It would, therefore, be highly desirable to find alternative and viable routes to retain or enhance the superior physical properties of the homopolymer PHB via melt compounding. The objective of the current study is consequently to study the feasibility of the melt blending nanocomposites route to yield property enhanced PHB materials.

Thus, the current study reports on the preparation and characterization of the morphology and barrier

properties of novel property enhanced nanobiocomposite blends of PHB with organically modified kaolinite and montmorillonite layered silicates and with PCL as a plasticizing element. A discussion about the polymer morphology and its thermal and barrier properties is also carried out at the light of the most commonly considered models for permeability reduction in nanocomposites.

EXPERIMENTAL

Materials

The bacterial PHB grade was purchased from Goodfellow Cambridge Limited, U.K., in powder form. The supplied PHB material with density 1.25 g/cm^3 is a melt-processable semicrystalline thermoplastic polymer made by biological fermentation from renewable carbohydrate feedstocks.

Polycaprolactone (PCL) grade FB100 was kindly supplied in pellet form by Solvay Chemicals, Belgium. This grade has a density of 1.1 g/cm^3 and a mean molecular weight of 100,000 g/mol.

A food contact complying phyllosilicate experimental grade (Nanoter^{TM} 2212) based on an organophilic surface modified kaolinite was kindly supplied by NanoBioMatters S.L., Spain. This grade was mainly used throughout the paper for generation of the biocomposites unless otherwise stated. A second food contact complying phyllosilicate experimental grade (Nanoter^{TM} 2000) based on an organophilic surface modified montmorillonite and designed for dispersion in polyolefins and polyesters was also supplied by NanoBioMatters S.L. No further details of sample preparation and modification were disclosed by the manufacturer.

Cloisite^{TM} 20A, a montmorillonite grade chemically modified with dimethyl, dihydrogenatedtallow $\sim$ 65% C18/$\sim$ 30% C16/$\sim$ 5% C14, quaternary ammonium salt was purchased from Southern Clay Products Incorporation, US.

Preparation of blends

Prior to the mixing step, the PBH and clays were dried at 70°C and the PCL at 45°C under vacuum for 24 h to remove sorbed moisture.

Neat PHB, PHB blends, as well as PHB nanocomposites were melt-mixed in an internal mixer (16 cm^3 Brabender Plastograph) during a mixing time of 6 min at a temperature of 182°C. The mixing was performed at a rotor speed of 60 rpm, which ensured that the melt temperature did not surpass 190°C at any moment during the mixing time. The batch was extracted from the mixing chamber manually and allowed to cool to room temperature in air. The resulting material was dried at 50°C at the above-mentioned conditions. The samples were finally transformed into sheets (0.7 and 0.1 mm thick) by compression molding in a hot-plate hydraulic press at 185°C and 2 MPa of pressure during 4 min. The polymer sheets were eventually allowed to cool to room temperature under pressure. All the measurements and experiments were carried out on these polymer sheets.

TABLE I
Description of the Samples Used

Samples code	Composition
PHB-blend	PHB/PCL, 80 : 20 wt/wt
4%NanoterPHB	4% wt of Nanoter^{TM} 2212 based on Kaolinite in neat PHB
1 or 4%NanoterPHB-Blend	1 or 4% wt of Nanoter^{TM} 2212 based on Kaolinite in PHB-Blend
4%NanoterMmtPHB-Blend	4% wt of Nanoter^{TM} 2000 based on montmorillonite in PHB-blend
4%CloisitePHB-Blend	4% wt of Cloisite^{TM} 20A based on montmorillonite in PHB-blend

The composition of the bioblends obtained in this work was (PHB/PCL) 100 : 0, term throughout the paper as PHB, and 80 : 20 wt/wt termed PHB-Blends. The clay loading of the nanobiocomposite samples was 1 and 4% wt/wt. Table I gathers the nomenclature and corresponding composition of the PHB nanocomposites used throughout the paper.

Oxygen transmission rate

The oxygen permeability coefficient was derived from oxygen transmission rate (OTR) measurements recorded using an Oxtran 100 equipment (Modern Control, Minneapolis, MN). During all experiments temperature and relative humidity were held at 24°C and 0%RH and at 24°C and 80%RH humidity. 80% relative humidity was generated by a built-in gas bubbler and was checked with a hygrometer placed at the exit of the detector. To avoid sample humidity equilibration during the actual oxygen transmission rate test at 80%RH and the subsequent fluctuations on barrier during the test, the samples were preconditioned at this RH by storage in a dessicator set up at this RH by appropriate salt solution. The experiments were done in duplicate at 0%RH an in quintuplicate at 80%RH, because the latter conditions are closer to real applications. As more data was accumulated at 80%RH, diffusion and solubility coefficients were also estimated at this humidity. The samples were purged with nitrogen for a minimum of 20 h, prior to exposure to a 100% oxygen flow of 10 mL/min, and a 5 cm^2 sample area was measured by using an in-house developed mask. Permeability

(P) and diffusion (D) coefficients were estimated from fitting the OTR-time curve to the first six sum terms of the following solution of the Fick's second law:[24]

$$\mathrm{OTR}(t) = \frac{P_p}{l}\left[1 + 2\sum_{n=1}^{\infty}(-1)^n \exp\left(-\frac{D\pi^2 n^2 t}{l^2}\right)\right] \quad (1)$$

In eq. (1), Pp is the oxygen partial pressure and l is the film thickness.

The diffusion coefficient can also be calculated using the ''half-time'' method and yielded no significant differences. In this method the diffusion coefficient can be estimated from the following equation:[25]

$$D = \frac{l^2}{7.1999 \cdot t_{1/2}} \quad (2)$$

where $t_{1/2}$ is the time for reaching an OTR value which is half that at the equilibrium.

Gravimetric measurements

Direct permeability to D(+)-limonene of 95% purity (Panreac Química, Spain) was determined from the slope of the weight loss-time curves at 24°C and 40% RH. The films were sandwiched between the aluminum top (open O-ring) and bottom (deposit for the permeant) parts of a specifically designed permeability cell with screws.[26] A Viton rubber O-ring was placed between the film and the bottom part of the cell to enhance sealability. Then the bottom part of the cell was filled with the permeant and the pinhole secured with a rubber O-ring and a screw. Finally, the cell was placed in the desired environment and the solvent weight loss through the film was monitored and plotted as a function of time. Cells with aluminum films were used as control samples to estimate solvent loss through the sealing. Cells clamping polymer films but with no solvent were used as blank samples to monitor water uptake. Solvent permeation rates were estimated from the steady-state permeation slopes. Organic vapor weight loss was calculated as the total cell loss minus the loss through the sealing and plus the water weight gain. The tests were done in duplicate.

The solubility and diffusion coefficients of D-limonene were estimated by gravimetry during desorption experiments at 24°C and 40%RH using an analytical balance Voyager® V11140 (Bradford, US). Thus, at saturation conditions, checked by observing no changes in successive weight uptake measurements of the specimens dipped in the aroma compound, the samples were thoroughly wiped with a tissue to remove the excess of aroma vapor condensed over the film surface (this step is considered as time zero) and were periodically weighted until they yielded constant weight. D values were obtained from fitting the experimental data versus time to the first six sum terms of the corresponding solution of Fick's second law [see eq. (3)] during desorption experiments.[27] Solubility was determined from equilibrium uptake measurements.

$$\frac{M_t}{M_e} = \frac{8}{\pi^2}\sum_{n=0}^{\infty}\frac{1}{(2n+1)^2}\exp\left\{\frac{-D(2n+1)^2\pi^2 t}{l^2}\right\} \quad (3)$$

In eq. (3), M_t is the sample weight at time t and M_e is the sample weight at saturation or equilibrium conditions.

FTIR measurements

Diffusion coefficients to water could not be determined by conventional gravimetric methods because of lack of sensitivity of the gravimetric method and were, therefore, alternatively determined by FTIR transmission spectroscopy during desorption from equilibrated specimens as described more in detail elsewhere.[27] To do so, the measuring chamber was continuously purged with a high flow rate stream of dry N_2 to maintain a zero concentration level of the vapors at the polymer film. During desorption, previously equilibrated samples were removed from the water, quickly wiped with a dry tissue to remove the excess of water vapor condensate from the surface, (this step is consider as time zero) and were immediately placed inside the measuring chamber to follow the desorption of the permeants. All FTIR experiments were carried out at 24°C and in duplicate. Diffusion coefficients were estimated by mathematical fitting of the desorption data to the first six sum terms of the corresponding solution of Fick's second law:

$$\frac{A_t}{A_e} = \frac{8}{\pi^2}\sum_{n=0}^{\infty}\frac{1}{(2n+1)^2}\exp\left\{\frac{-D(2n+1)^2\pi^2 t}{l^2}\right\} \quad (4)$$

In eq. (4), A_t and A_e are the absorbances (OH stretching band centered at 3400 cm^{-1}) at a given time t and at saturation or equilibrium sorption conditions, respectively.

DSC measurements

Differential scanning calorimetry (DSC) of PHB and its biocomposites was performed on a Perkin-Elmer DSC 7 (Waltham, MA) thermal analysis system on typically 7 mg of material at a scanning speed of 10°C/min from room temperature to the melting point using N_2 as the purging gas. Before evaluation, the thermal runs were subtracted analogous runs of

an empty pan. The crystallinity of the samples was estimated using as the heat of fusion for an infinity crystal of PHB 146 J/g[28] and for this of PCL 136 J/g.[29] The DSC equipment was calibrated using indium as a standard.

SEM measurements

For scanning electron microscopy (SEM) observation, the samples were fractured in liquid nitrogen and mounted on bevel sample holders. The fracture surface of the different samples was sputtered with Au/Pd in a vacuum. The SEM pictures (Hitachi S4100) (Hitachi High Technologies, Wokingham, UK) were taken with an accelerating voltage of 10 keV on the sample thickness.

TEM measurements

Transmission electron microscopy (TEM) was performed using a JEOL 1010 (Jeol, Tokyo, Japan) equipped with a digital Bioscan (Gatan) image acquisition system. TEM observations were performed on ultra-thin sections of microtomed thin biocomposite sheets.

X-ray experiments

Wide angle X-ray experiments (WAXS) were performed using a Siemens D5000D equipment (Germany). Radial scans of intensity versus scattering angle (2θ) were recorded at room temperature in the range 2 to 28°(2θ) (step size = 0.03°(2θ), scanning rate = 8 s/step) with identical settings of the instrument by using filtered Cu Kα radiation (λ = 1.54 Å), an operating voltage of 40 kV, and a filament current of 30 mA. To calculate the clay basal spacing Bragg's law (λ = 2d sin θ) was applied.

Statistical analysis

One-way analysis of variance (ANOVA) was performed using XLSTAT-Pro (Win) 7.5.3 (Addinsoft, NY). Comparisons between treatments were evaluated using the Tukey test.

RESULTS AND DISCUSSION

Morphological results in PHB-Kaolinite nanocomposites

Figure 1 shows SEM pictures from some of the samples taken using three different magnifications. From this Figure it can be seen that the PHB-Blend contains a very fine dispersion of the PCL phase in the matrix. Albeit, some debonding is observed at the polymer interphase, a closer inspection of the phase morphology shows that there is interfacial adhesion between the dispersed PCL phase and the biopolymer matrix. The two polymers are, therefore, not miscible as further suggested by observation of two melting points at around the same temperature as in the neat components (see later), but somewhat compatible due to the observed interfacial contact. A similar two phase morphology is also observed for the 4%NanoterPHB-Blend. However, for this particular sample, additional phases displaying clay particles or aggregates are not discernible from the SEM pictures, suggesting that the clay may be well dispersed across the polymer morphology. On the other hand and unlike the latter 4%NanoterPHB-Blend, the 4%NanoterPHB sample (with no PCL) does clearly exhibit a highly dispersed but irregular in size two-phase morphology, where clay particles can be easily spotted across the biopolymer matrix. A closer inspection into this sample [See Fig. 1(D,G)] indicates the presence of some mineral aggregates, i.e. tactoids, ranging in size from few tens of nanometers up to about one micron in thickness with some apparent weak adhesion at the interphase. Surprisingly and as stated earlier, this segregated morphology is not seen in the biocomposite containing kaolinite clay and PCL. It would appear, from the SEM pictures, as if the organomodified clay could be more easily compatibilized and dispersed during blending in the presence of this more viscoelastic blending component. The reason for this could be related to a better dispersion of the clay in the PCL phase or/and to the particular melt stabilization that the PCL component induces to the blend as will be later derived from the DSC experiments.

Figure 2 shows the WAXS patterns of the above samples and, additionally, it shows the diffraction patterns of the 1%NanoterPHB-Blend and of the unmodified (raw clay) and surface modified kaolinite (Nanoter™ 2212) based clays. From this figure, it can be easily seen that the modified clay shows a dominant (001) diffraction peak at angle 7.8° indicating that the intergallery or basal space of the natural clay with peak at 12.4° has been expanded from 0.7 nm up to, at least, 1.13 nm as a result of the organic modification and that most of the natural clay has undergone the intercalation. On the other hand, in the diffractograms of the biocomposites in Figure 2, only one clay peak can be discerned, which is located at about the same position as in the unmodified clay; no clay peak is, however, discerned in the 1%NanoterPHB-Blend. These observations indicate that during the melt mixing process, partial or total clay agglomeration or platelet collapse has taking place within the polymer matrix for the samples with 4% Nanoter™ 2212 loadings, due to probably losses of surfactant at the clay surface during the relatively extensive mixing cycle. In spite of that, the presence of the natural clay peak is clearly stronger

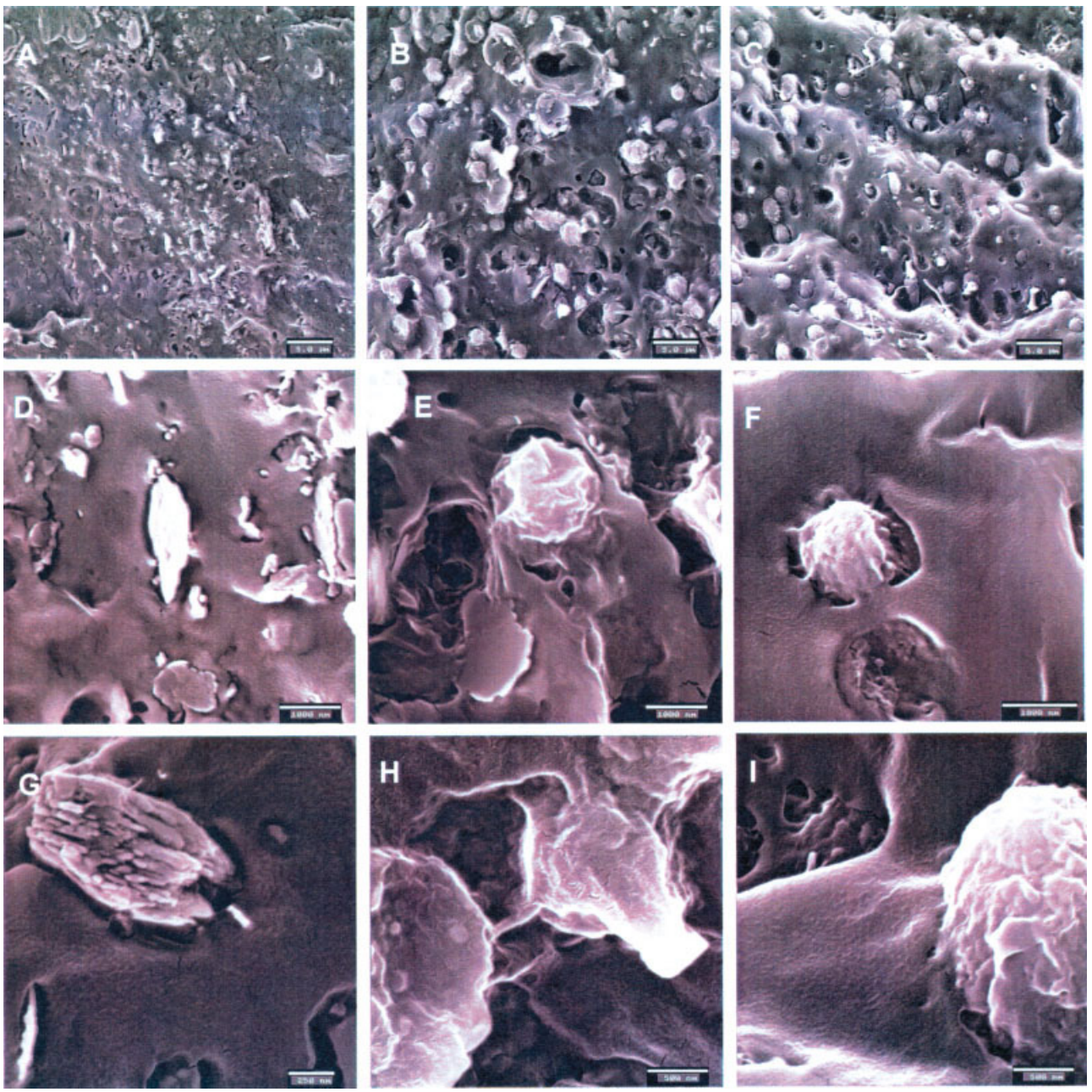

Figure 1 SEM pictures with increasing magnification of the samples 4%NanoterPHB (A, D, and G with scale markers of 5 μm, 1 μm, and 250 nm, respectively), 4%NanoterPBH-Blend (B, E, and H showing scale markers of 5 μm, 1 μm, and 500 nm, respectively), and PHB-Blend (C, F, and I with scale markers of 5 μm, 1 μm, and 500 nm, respectively). [Color figure can be viewed in the online issue, which is available at www.interscience.wiley.com.]

(and at exactly the same position as in the natural clay) in the 4%NanoterPBH sample than in the 4%NanoterPBH-Blend sample, suggesting that a better dispersion of the organomodified clay may have been achieved through the use of the PCL component in the blends. Of course, it is difficult to discriminate how much of the originally modified clay has agglomerated and how much has been dispersed (intercalated or/and exfoliated) in any of the samples because there is no internal standard. Nevertheless, from the comparative intensity and shape of the clay peaks in Figure 2, from the SEM results and from the TEM results that follow it seems reasonable to assume that a fraction of the clay has been, at the least, intercalated within the polymer matrix. Thus, from the above, it is inferred that a better compatibilization of the organomodified clay with the PHB/PCL blend occurs. The sample with 1% clay loading could, however, be even more dispersed in the matrix since no trace of clay peak is observed in Figure 2.

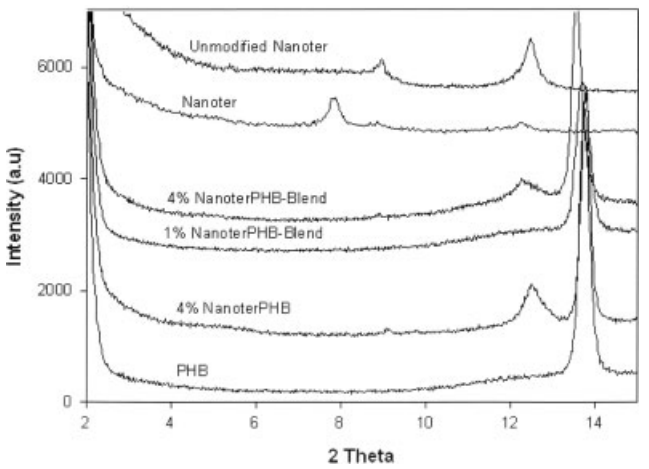

Figure 2 X-ray diffractograms of the unmodified (raw mineral) and modified kaolinite clays and of the various PHB nanobiocomposites.

Overall, the WAXS results point again that the NanoterPHB-Blends seem to have a more favorable morphology in terms of dispersion than the NanoterPHB samples.

Figure 3 shows some TEM results taken on specimens of the 4%NanoterPHB-Blend and 1%NanoterPHB-Blend. This figure indicates that the former sample displays a highly dispersed irregular morphology consisting of intercalated thin tactoids with different sizes and some completely exfoliated (see white arrows) layered clay particles of different size and platelet orientation. Interestingly, it is observed that the smaller clay particles appear also fractured, whereas the intercalated particles are more prone to remain in larger sizes in the platelets direction. Regarding particle aspect ratio, it is difficult to estimate accurate values given the dispersion in sizes, platelet shape, and particles orientation, but the lowest aspect ratios (L/W) that were estimated from the pictures are for the biggest particles and ranges from around 8 to 40. A combination of appropriate surface modification and sufficiently high shear forces in the melt during polymer processing is usually required to generate extensive ratios exfoliation/intercalation in nanocomposites; however, fully exfoliated systems are very seldom achieved via conventional melt blending routes in thermoplastic polyesters. The sample 1%NanoterPHB-Blend appears to show, however, more dispersed clay morphology, in which some exfoliated platelets (white arrows) and some intercalated laminates can be observed.

Thermal properties of PHB-Kaolinite nanocomposites

The crystallinity and melting point of the blends were measured by DSC and the results are gathered

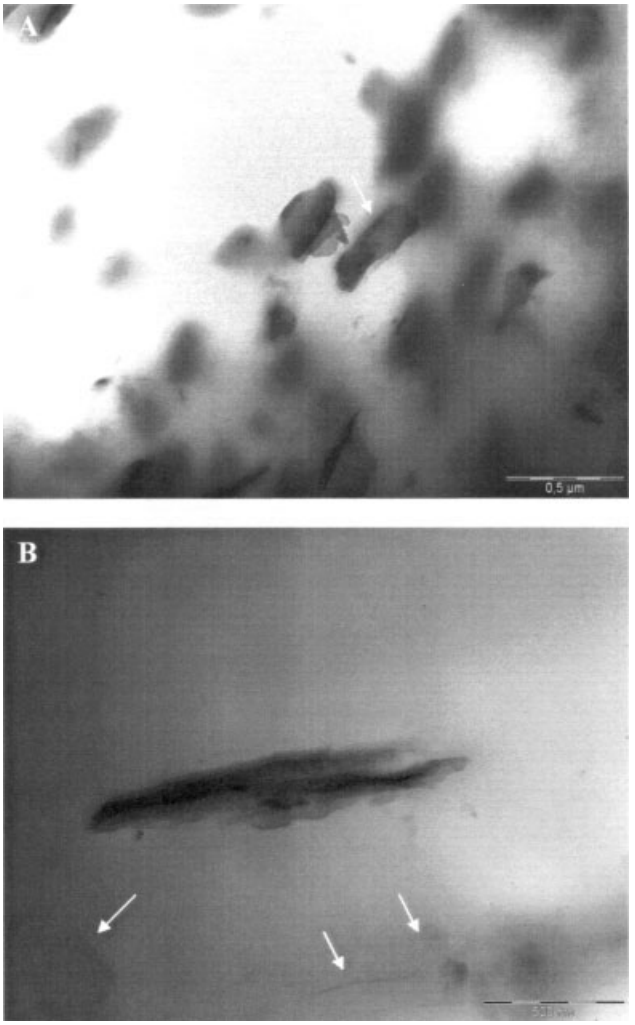

Figure 3 TEM pictures of 4%NanoterPHB-Blend sample (A showing scale markers of 0.5 µm) and of 1%NanoterPHB-Blend sample (B with scale markers of 0.5 µm).

in Table II. From this table, it can be seen that the melting point is not greatly altered in the clay containing samples but that the crystallinity (corrected for the biopolymer content in the composite) increases. The latter result adds to similar nucleating observations reported in previous works for PHB/

TABLE II
DSC Melting Point and Melting Enthalpy of the Samples

Sample	M_p (°C)	PHB melting enthalpy (J/g)	PHB crystallinity (%)
PHB-Blend	176 (64)	93 (60)	64 (44)
4% NanoterPHB-blend	175 (65)	99 (53)	68 (39)
PHB	175	94	64
4% NanoterPHB	175	103	71
PCL	62	52	38

The values for the PCL fraction in the blend are given between brackets.

HV nanocomposites,[23] and suggests that the clay can act as a heterophase nucleating agent, hence promoting higher crystallinity in the matrix. In spite of that, Table II suggests that the melting point is either not affected or is slightly reduced (see later Fig. 7) for the more dispersed 4%NanoterPHB-Blend. Changes in melting point are the result of many factors such as changes in molecular orientation, crystal thickness, and crystal perfection. An increase in the latter factors leads to increased melting points.[30] Nevertheless, despite the fact that the crystallinity goes up in the nanocomposites the melting point is either unaffected or slightly reduced. A reduction in crystal size could explain a small decrease in melting point, but also some polymer degradation and chain scission due to melt processing.[13] It should be borne in mind that the natural PHB homopolymer used is a nonstabilized material which is even more unstable than commercial formulations of this or than PHBV copolymers. Albeit, the changes in the melting point of the samples are probably not meaningful because they are very small and, perhaps, within the experimental error of the technique, interestingly, the PHB-Blend appears to show slightly higher melting point than the neat PHB. This may indicate that the PCL plasticizing phase component could tend to act as a stabilizing agent for the biopolymer. In light of the cited previous work,[13] which indicated that processing of PHB should be carried at temperatures below T_m + 15°C to avoid polymer degradation, the samples were not allowed to surpass during melt mixing 190°C by using a relatively low torque during processing. Of course, the use of a relatively low processing torque has a drawback that the impairment in the ability of the systems to exfoliate further due to the lower shear forces generated in the melt.

More evident support to prove the instability of the homopolymer PHB arises from the crystallization and remelting behavior of the samples. Thus, further DSC crystallization experiments obtained by cooling at 10°C/min the fresh molten samples after 1 min in the melt at 188°C in the presence of a nitrogen purge, indicated that the crystallization temperature (T_c) for the PHB-Blend specimen was 121.0°C, but for the 4%NanoterPHB-Blend it became 112°C. This decrease in the crystallization point of the blend strongly suggests that thermal exposure of the nanobiocomposites results in lower crystallization rate due to most likely molecular degradation and further decrease in molar mass and, subsequent, depletion in nucleation density.[13] Further, degradation with successive heating cycles is revealed by data gathered after a second heating run at 10°C/min following crystallization of the samples. These results yielded for the PHB-Blend a melting temperature of 175.7°C and a crystallinity for the PHB fraction of 63% and for the 4%NanoterPHB-Blend a melting temperature of 173.4°C and a crystallinity for the PHB fraction of 57%. As a result, the nanocomposite blend shows with increasing thermal aging, even in the presence of an inert gas, a much larger decrease in melting point compared to data gathered for the first heating of the sample in Table II, but also a decrease in melting enthalpy with extensive thermal exposure in accordance with results and degradation behavior reported earlier. This behavior is most likely related to a filler assisted acceleration in thermal degradation for the polymer. Since, the mechanism of degradation for this biopolymer is thought to occur by esterification reaction between hydroxyl and carboxyl groups,[13] and as clay particles are inorganic hard particles which furthermore exhibit some hydroxyl and other potentially reactive moieties and impurities, the effect of a highly disperse filler may consequently be to facilitate the latter chemistry or other chemical and/or chain scission mechanisms (see later in the paper).

PHB-montmorillonite nanocomposites

In view of the above results and since more aggressive processing conditions were precluded in the internal mixer, an alternative route of blending with higher intergallery swollen clay systems was considered to aim fully exfoliated morphologies. It is well reported that organomodified montmorillonite has a higher intergallery spacing, even as a natural clay, compared to kaolinite and, therefore, it should in principle be more easily dispersible within the polymer matrix.

In this context, further blending of PHB was similarly carried out with 20% (w/w) of PCL but alternatively with a 4% wt of Cloisite 20A and with a 4% Wt of a highly swollen organophylic montmorillonite (Nanoter 2000) (see Table I). Figures 4 and 5 show SEM and TEM results of these nanocomposites and Figure 6 shows the WAXS diffraction patterns of the composites and of the two commercial clays. Surprisingly, nanocomposites with both of the above clay systems yielded extremely soft and fragile materials with hardly any mechanical consistency suggesting that these organophylic montmorillonite grades under the same blending conditions undergo extensive molecular degradation (see DSC and ATR-FTIR results below).

Figure 4 reveals that the SEM morphology of both nanocomposites is coarser and flaky at the fracture surface compared to that of the unfilled blend. This particular microscopic discontinuous morphology is responsible for the macroscopic spongy and soft character of the material. However, no filler particles can be seen, fact that indicates that a good dispersion of the clay must have been achieved in both systems. Figure 5 shows some TEM pictures of the

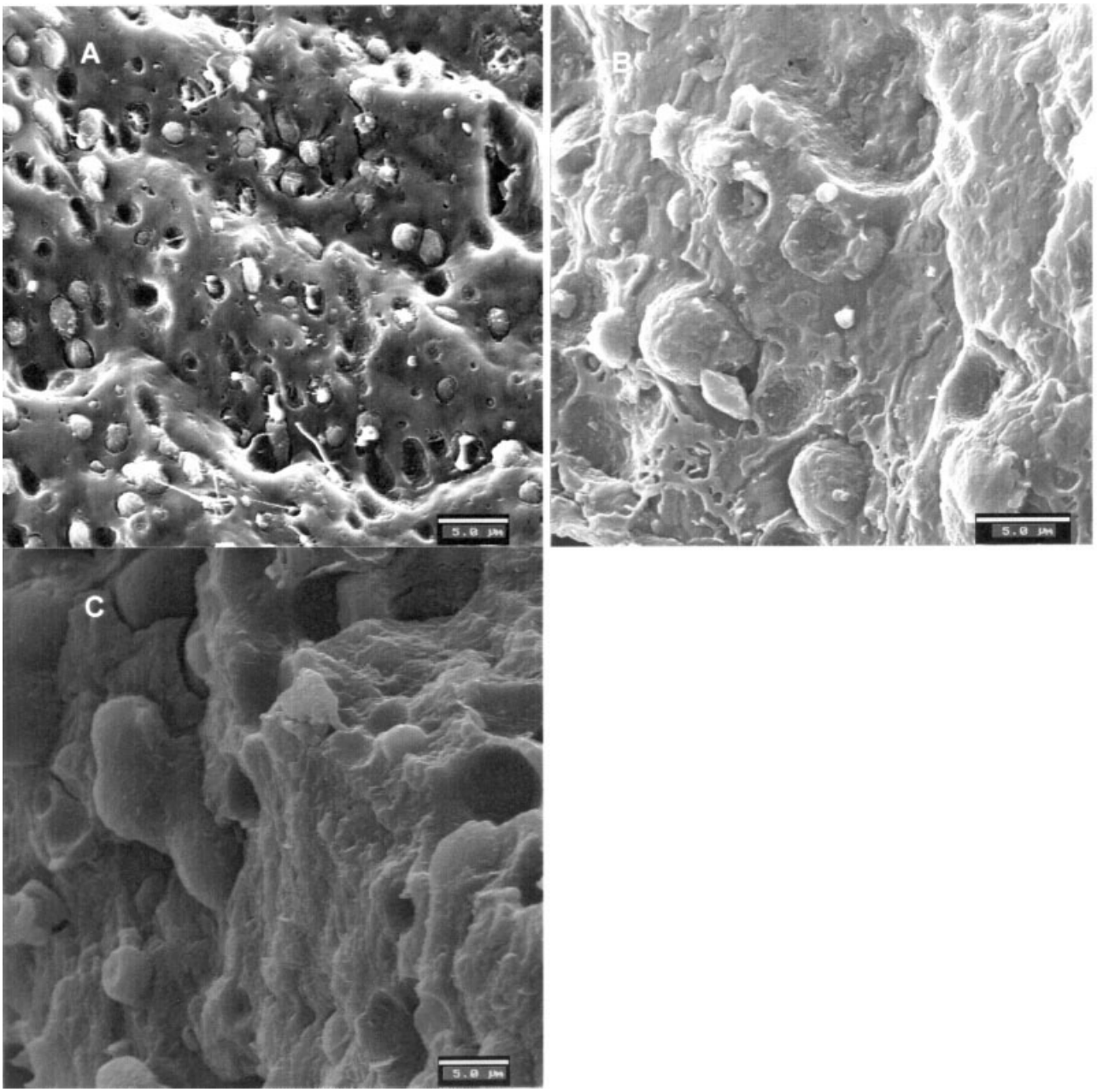

Figure 4 SEM pictures of samples PHB-Blend (A), 4%CloisitePHB-Blend (B), and 4%NanoterMmtPHB-Blend (C). The pictures show scale markers of 5 μm.

4%CloisitePHB-Blend revealing the presence of larger length (due to the higher aspect ratio of the montmorillonite) in layers of apparently nonoriented clay particles, which are more highly dispersed across the polymer morphology than was observed in Figure 3, although still the system does not show a fully exfoliated morphology. Nanometric thin clay platelets can, however, be clearly discerned to be randomly dispersed across the polymer matrix.

Interesting observations are also derived from the X-ray patterns in Figure 6: In the montmorillonite based samples, while Cloisite 20A clay shows an intergallery spacing of d_{001} = 24.6 Å, the Nanoter Mmt grade shows a spacing of d_{001} = 39.40 Å, indicating that the latter clay is more effectively swollen or expanded. Other two peaks, besides the most intense one at 2θ 2.3°, are observed at angles 4.6° and 6.9°, which are associated to the second and third order diffraction features, respectively. This highly ordered and stacked layered modified structure should of course lead to more easily dispersable clay morphologies in polymers and biopolymers, and further work is being carried out at present to evaluate its capacity to design more advanced nanocompo-

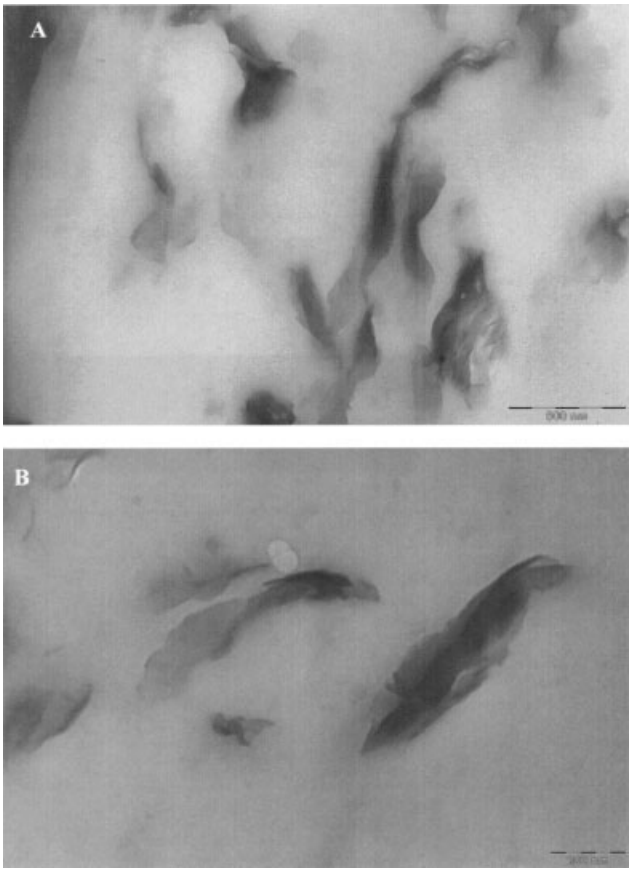

Figure 5 TEM picture of the 4%CloisitePHB-Blend. Scale markers are 0.5 μm for picture A and 0.2 μm for picture B.

sites. Figure 6 clearly indicates that in neither of the nanobiocomposites the clay peaks are discerned, suggesting again that a good clay dispersion across the biopolymer matrix must have been achieved for both systems. Nevertheless, it is worth noting that even when no clay basal peak is observed in the diffractograms of the nanobiocomposites in Figure 6, not fully randomly dispersed exfoliated morphologies are suggested by the TEM experiments. As a result, caution should be taken when assumptions are made regarding the existence of randomly dispersed platelet systems on the sole bases of lack of basal peaks in the X-ray experiments.

Finally, Figure 7(a) shows the DSC melting thermograms of the unfilled and filled nanocomposites revealing melting features of both the PCL, at $\sim 60^{\circ}$C, and the PHB, at $\sim 176^{\circ}$C, fractions. From this figure, the two composites containing montmorillonite exhibit a multiple melting endotherm (with two peaks) of noticeable lower melting point than both the unfilled blend and their kaolinite counterparts, suggesting that most likely extensive degradation of the PHB matrix has taken place during compounding with these particular clays. This is further substantiated by the ATR-FTIR spectra plotted in Figure 7(b).

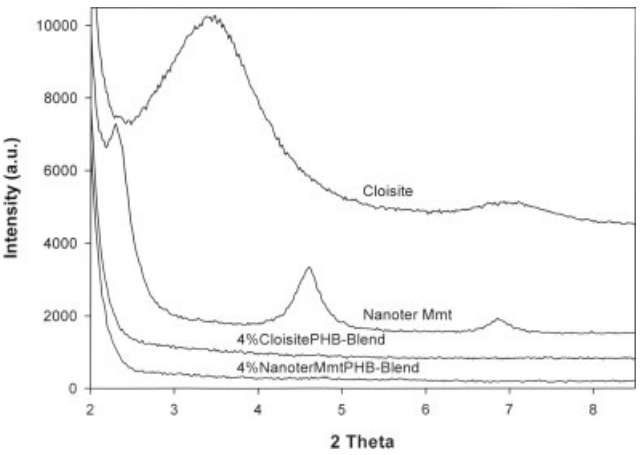

Figure 6 X-ray patterns of two montmorillonite-based surface modified clays and of their correspondent PHB-Blend biocomposites.

Figure 7(b) indicates that clear differences can be seen between the PHB-Blend and its nanocomposites depending on whether organomodified kaolinite or

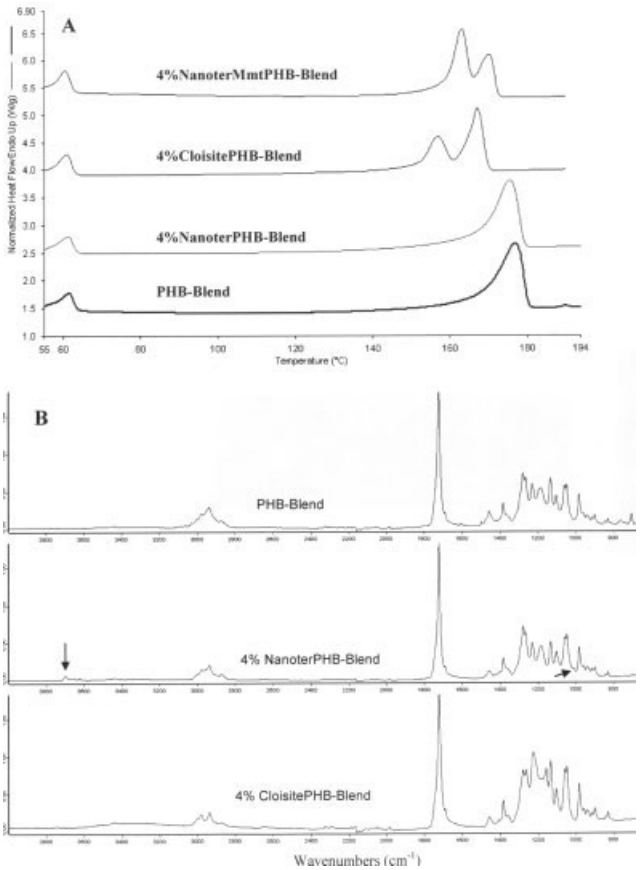

Figure 7 (A) DSC melting endotherms of from top to bottom, 4%NanoterMmtPHB-Blend, 4%CloisitePHB-Blend, 4%NanoterPHB-Blend, and PHB-Blend. (B) ATR-FTIR spectra of from top to bottom, PHB-Blend, 4%NanoterPHB-Blend, and 4%CloisitePHB-Blend. The arrows indicate the presence of clay peaks in the middle spectrum.

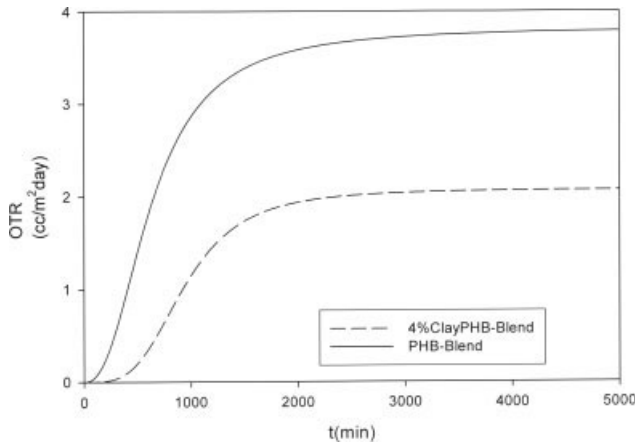

Figure 8 Oxygen transmission rate curve of the PHB-Blend and of the 4%NanoterPHB-Blend.

montmorillonite clays are used. In the 4%NanoterPHB-Blend, there are some peaks, i.e. at 1008 and 3700 cm^{-1}, which arise from the presence of the clay in the blend (see arrows). However, by comparison of the latter sample with the PHB-Blend there are some spectral changes such as the disappearance of a band at 700 cm^{-1} and some small changes in the relative intensity of bands in the range from 1000 to 1500 cm^{-1} and in the group of bands around 2950 cm^{-1}. On the other hand, much bigger and different alterations are observed for the 4%CloisitePHB-Blend sample (the strong montmorillonite peak at 1008 cm^{-1} is not discernible in the spectrum). This sample shows large spectral variations in the band envelop from 1000 to 1500 cm^{-1}, which clearly point to, at the least, chemical alterations in the material. More recent work making use of gel permeation chromatography measurements (GPC) and other techniques carried out in this and in PHBV nanocomposites indicated strong molecular weight decrease, particularly in the presence of organomodified montmorillonite clays (will be published elsewhere). All of these changes strongly point to the hypothesized molecular degradation mechanism, most notably in the 4%CloisitePHB-Blend, and molecular weight reductions. The particular degradation behavior for the montmorillonite nanocomposites could be related to the different nature of the clay, e.g., sorbed water, specific clay surface chemistry and higher aspect ratio but it is probably also related to the higher degree of molecular dispersion achieved for these particular systems, which promotes a more intimate contact between clay and polymer.

Mass transport properties of PHB-Kaolinite nanocomposites

Figure 8 shows, as an example, the oxygen transmission rate curves at 0%RH of the 4%NanoterPHB-Blend and of the unfilled PHB-Blend. From this Figure, it is seen that the equilibrium transmission rate is higher in the unfilled blend than in the nanocomposite indicating that a lower permeability is reached in the nanocomposite systems, and that the diffusion appears faster in the unfilled blend. Table III shows the oxygen permeability coefficients at dry (0%RH) and at 80% RH for the various samples. From this Table III, it is seen that the oxygen permeability is most largely reduced, i.e. by $\sim$ 43%, at 0%RH in the 4%NanoterPHB-Blend compared to the 4%NanoterPHB sample. This supports the morphology data discussed earlier, which displayed a more dispersed morphology for the composite containing PCL. The 1%NanoterPHB-Blend shows a permeability reduction at 0%RH of $\sim$ 10%. Table III also shows that at a higher relative humidity, i.e. 80%RH, the oxygen barrier is somewhat lower in the neat polymer compared to dry conditions; however, increasing RH

TABLE III
Oxygen Permeability of the Various Samples at 0% RH and at 80% RH and Estimated Diffusion and Solubility Coefficients at 80% RH for the Blends

Sample	PO_2 (m^3 m/m^2 s Pa) 24°C, 0% RH	PO_2 (m^3 m/m^2 s Pa) 80% RH	DO_2 (m^2/s) 80% RH	SO_2 (m^3/m^3 Pa) 80% RH
PHB-Blend	$^{a}4.2 \pm 0.0005\ e^{-19}$ ($14.6\ e^{-19}$) ($4.0\ e^{-19}$)	$^{a}5.2 \pm 0.004\ e^{-19}$	$^{a}1.1 \pm 0.01\ e^{-12}$	$^{a}4.7 \pm 0.05\ e^{-7}$
1%NanoterPHB-Blend	$^{b}3.8 \pm 0.3\ e^{-19}$	$^{b}3.9 \pm 0.1\ e^{-19}$	$^{b}1.0 \pm 0.02\ e^{-12}$	$^{b}3.9 \pm 0.2\ e^{-7}$
4%NanoterPHB-Blend	$^{c}2.4 \pm 0.3\ e^{-19}$	$^{c}2.8 \pm 0.2\ e^{-19}$	$^{c}0.8 \pm 0.01\ e^{-12}$	$^{c}3.5 \pm 0.3\ e^{-7}$
PHB	$^{A}2.3 \pm 0.002\ e^{-19}$	–	–	–
4%NanoterPHB	$^{B}1.8 \pm 0.3\ e^{-19}$	–	–	–
PCL	$58.0\ e^{-19}$	–	–	–
PET	$3.3\ e^{-19}$	$3.8\ e^{-19}$		

The permeability of a PET commercial film measured under the same conditions is also reported for comparison purposes. The a, b, and c and A and B letters correspond to the ANOVA statistical analysis of the data that indicate that with a 95% level of confidence the values are significantly different.

Value 14.6 e−19 in second row of column 2 is calculated using the rule of mixtures.

Value 4.0 e^{-19} in third row of column 2 is calculated using the model of Maxwell as extended by Roberson.

does not seem to enhance so apparently the oxygen permeability of the composites compared to their performance in dry. At 80%RH a 46% decrease in oxygen permeability is observed in the filled blend compared to the unfilled material, which is slightly higher than that measured at 0%RH.

From an applied view point, Table III also teaches that although the PHB blend has higher permeability than both the neat PHB and petroleum-based amorphous polyethylene terephthalate (PET), the 4% clay loaded nanocomposite clearly maintains the barrier of the neat PHB polymer and outperforms the barrier properties of PET at dry and at high relative humidity conditions.

Figure 9 shows examples of the application of the Nielsen and Fricke models [eq. (2)] to different aspect ratios (W/L) of layered particles. The model of Nielsen[31] [see eq. (5)] and other ulterior refinements such as the one of Fredrickson and Bicerano,[32] describe systems in which the layered i.e., thin, flat, and squared particles are perfectly oriented with length and width perpendicular to the permeant transport direction and are homogeneously diluted in the polymer matrix.

$$\frac{P_{\text{nano}}}{P_{\text{neat}}} = \frac{1 - V_{\text{clay}}}{1 + (L/2W)V_{\text{clay}}} \tag{5}$$

In eq. (1), L/W is the aspect ratio of the platelets and V_{clay} the volume fraction of the clay filler.

The model of Fricke[33] describes oblate randomly oriented spheroids uniformly distributed across the matrix [see eqs. (6) and (7)].

$$\frac{P_{\text{nano}}}{P_{\text{neat}}} = \frac{1 - V_{\text{clay}}}{\tau} \tag{6}$$

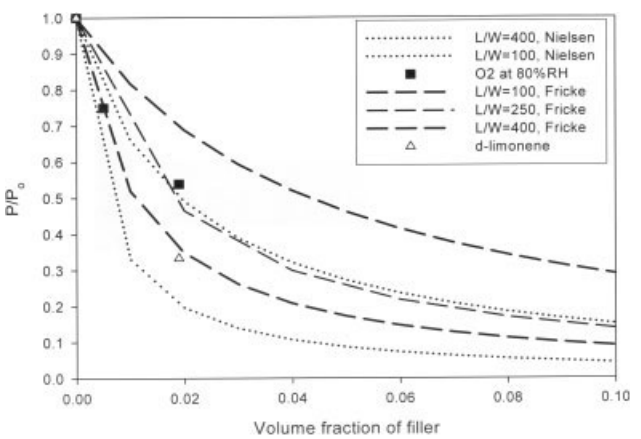

Figure 9 Experimental permeability data of the PHB-Blends to oxygen at 80%RH and D-limonene and, theoretical, permeability versus filler content curves resulting from application of the formalisms of Nielsen and Fricke to several clay platelet aspect ratios.

$$\frac{W}{L} = \frac{1}{0.785 - \sqrt{0.616 - \frac{V_{\text{clay}}/(\tau-1)}{(V_{\text{clay}}/(\tau-1))+3}}} \tag{7}$$

In eq. (6), τ is the tortuosity factor, which increases with increasing impedance efficiency of the clay filler. Equation (7) relates within this model the volume fraction of clay and the aspect ratio to the tortuosity factor.

Figure 9 additionally plots the experimental oxygen permeability data measured at 80%RH. The results seem to best fit the Nielsen model for aspect ratios of the layered particles around 100, and the Fricke model for particles of aspect ratios around 250. However, the best fitting to these models appear to overestimate the actual aspect ratio of the particles morphology, at least this of the biggest ones, as observed by TEM in Figure 3. Thus, it should be taken into account that there are a number of morphological factors that these simple models obviate. The main factors disregarded, besides the fact that these particles are not perfectly aligned or completely random, are the morphological changes in the matrix or blending components (mainly crystallinity, crystalline morphology, relative humidity effect, molecular degradation and molar mass reduction, and amorphous and interfacial changes) and do not account for heterogeneity in the aspect ratio of the filler experimentally observed in Figure 3.

Another interesting observation from Table III is that the permeability of the unfilled PHB-Blend is lower than that expected from application of the simple rule of mixtures of the pure PHB and PCL components; however, this approaches more closely the permeability value predicted by application of the model of Maxwell as extended by Robertson [see eq. (8)].[34,35]

$$P_{\text{Blend}} = P_{\text{PHB}}\left[\frac{P_{\text{PCL}} + 2P_{\text{PHB}} - 2V_{\text{PCL}}(P_{\text{PHB}} - P_{\text{PCL}})}{P_{\text{PCL}} + 2P_{\text{PHB}} + V_{\text{PCL}}(P_{\text{PHB}} - P_{\text{PCL}})}\right] \tag{8}$$

Equation 8 describes the permeability of blend systems in which both matrix (PHB) and blending components (PCL) are permeable, and in which the blending component are spheres evenly distributed across the matrix as is observed from Figure 1(C,F,I).

Table III also shows the estimated diffusion and solubility coefficients for the blends at 80%RH. The solubility coefficient was easily derived from the well-known simple relation $P = DS$. The estimated diffusion and solubility coefficients are seen to decrease in the composites with the incorporation of clay and with increasing clay content in the matrix as expected. In the case of diffusion, the presence of platelets is thought to increase the tortuosity (τ) or detour factor in the materials leading to slower dif-

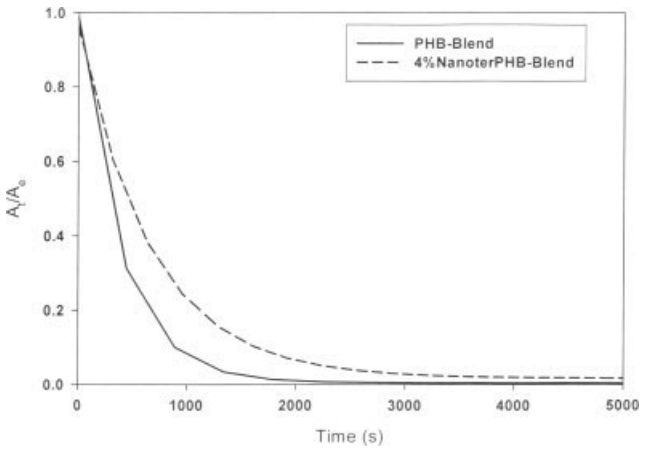

Figure 10 Water desorption curves as follow by FTIR versus time for PHB-Blend and for 4%NanoterPHB-Blend film specimens.

fusion processes and, therefore, to lower permeability. Nevertheless, the diffusion coefficient is seen to be reduced by only 27%, whereas the permeability is reduced by 46%. Therefore, the solubility parameter must also have a significant role in the biocomposites. The solubility coefficient is indeed seen to decrease from observation of Table III. However, the solubility decrease is higher than would be expected from simple application of eq. (9).

$$S_{\text{nano}} = S_{\text{neat}}(1 - V_{\text{clay}}) \tag{9}$$

In this equation, S_{nano} means solubility of the nanocomposite, S_{neat} solubility of the matrix, and V_{clay} is the volume fraction of clay. The equation is derived from eqs. (5) or (6), which subsequently derived from the well-known solubility model developed for semicrystalline polymers in which a solubility decrease is expected to occur with increasing the crystallinity fraction (Ref. 7 and therein; Ref. 25). Thus, while only $\sim$ 0.5 and 2% reductions in solubility would be expected for 1 and 4% wt/wt of clay loadings, the experimental reduction values are of 17 and 25%, respectively. The latter results highlight that simple models cannot be applied to describe complex systems such as those described in the paper, in which morphological changes, molar mass reduction, polymer degradation, relative humidity, and crystallinity increase factors take place.

Figure 10 shows water desorption curves of unfilled and filled blends as obtained from FTIR spectroscopy data recorded during desorption from equilibrium saturation conditions. From the data in Figure 10, a diffusion coefficient can be easily estimated which is gathered in Table IV. From this table, the diffusion coefficient of water in the biocomposite is seen to be reduced by $\sim$ 72% compared to the unfilled polymer blend during desorption. Nevertheless, the

TABLE IV
Water Diffusion Coefficient as Determined by FTIR and D-Limonene Direct Permeability, Diffusion, and Solubility Coefficients as Determined by Gravimetry in the Blends

Sample	PHB-blend	4% Nanoter PHB-blend
D_{Water} (m^2/s)	[a]1.1 ± 0.08 e^{-17}	[b]0.3 ± 0.04 e^{-17}
P_{Limonene} (kg m/m^2 s Pa)	[a]0.9 ± 0.05 e^{-15}	[b]0.3 ± 0.1 e^{-15}
D_{Limonene} (m^2/s)	[a]0.02 ± 0.002 e^{-10}	[b]0.008 ± 0.001 e^{-10}
S_{Limonene} (kg/kg Pa)	[a]1.13 ± 0.16 e^{-5}	[b]1.44 ± 0.11 e^{-5}

The a and b letters correspond to the ANOVA statistical analysis of the data that indicate that with a 95% level of confidence the values are significantly different.

solubility was seen to increase in the composite blend. Thus, the FTIR band area of the water band at 3400 cm^{-1} corrected for sample thickness (A_{3400}/L (μm)) was found to be 1.95 for the PHB-Blend, whereas for the 4%NanoterPHB-Blend was 3.00. This means that the nanocomposite uptakes $\sim$ 54% more water than the unfilled blend due to likely the existing hydrophilic sites of the filler. On the whole, as the water permeability is the product of D and S, this meaningful transport parameter is expected to be lower since the reduction in diffusion is seen larger than the 54% increase in solubility.

Figure 11 shows limonene weight loss experiments for the two blends. From the slope of such curves, direct permeability results can be easily derived that are presented in Table IV. Table IV also presents the estimated diffusion coefficient of limonene and its solubility coefficient as determined by weight uptake measurements for the blends. From the results, a

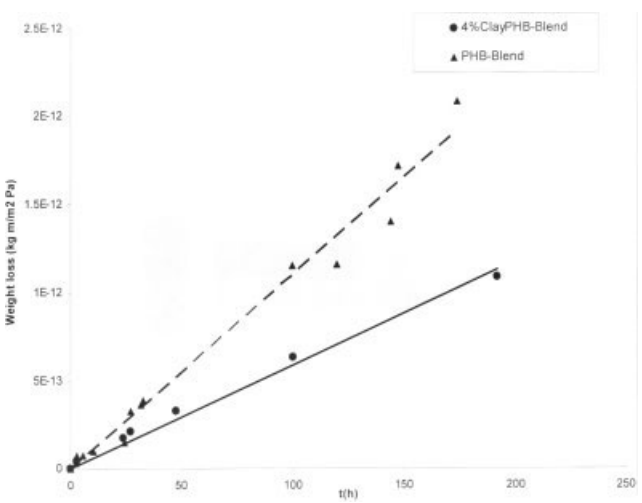

Figure 11 D-limonene direct permeability (weight loss versus time) results for PHB-Blend and for 4%NanoterPHB-Blend film specimens.

reduction in permeability of $\sim$ 67% and in the diffusion coefficient of 60% is observed in the biocomposite for this particular organic vapor. On the other hand, the limonene solubility shows the opposite behavior and increases in the nanocomposite by $\sim$ 27%. This is likely the result of the affinity of the organophylic sites of the filler for this less hydrophilic component. Figure 9 also plots the permeability decrease for this component versus the modeling work. From the modeling work a higher barrier effect compared to that for oxygen is observed which is best described in the model of Fricke by an aspect ratio of about 400.

Overall, the biocomposites exhibit increased gas, aroma, and water vapor barrier performance. However and in accordance with previous works,[36,37] the barrier effect was seen to be penetrant dependent. Conversely, these barrier results are in disagreement with most commonly considered models which simply relate permeability reduction to filler shape and volume fraction. In the above experiments, the tortuosity factor related to the diffusion process appears to be larger for the vapor interacting molecules, which on the other hand have increased solubility as expected.

CONCLUDING REMARKS

This article reports morphology data, thermal, and barrier properties of novel nanobiocomposites comprising PHB, PCL as plasticizing element and three commercial organomodified clays based on kaolinite and montmorillonite phyllosilicates. PHB is known to be a very rigid and melt unstable material; however, it does exhibit somewhat better oxygen barrier than its petroleum based counterpart PET.[38] Thus, the underlying objective of this work was to provide an understanding for the relation between structure and properties for nanocomposites of PHB and to develop novel PHB composites with enhanced barrier properties of interest in rigid food packaging applications for food and beverage trays and containers. From the results, it was found that indeed nanocomposites of PHB with highly swollen clay systems (based on montmorillonite) led to highly dispersed morphologies in the biopolymer. However, the montmorillonite systems simultaneously resulted in extremely soft materials of probably no use in most packaging applications because of extensive polymer degradation of the biopolymer as suggested by DSC and ATR-FTIR results. Similar nanocomposites with a less swollen organomodified clay (based on kaolinite) led to a less dispersed and irregular morphology. Surprisingly, this characteristic was found to generate a novel biomaterial with enhanced crystallinity and barrier properties, due to the clay reinforcing effect.

The addition of the PLC to the PHB was found to lead to a nonmiscible but compatible interphase blend, and this component appeared to increase compatibilization with the organophylic clay.

The barrier properties of the systems were not seen to fit the most widely applied models such as those of Nielsen and Fricke for oriented and random dispersion of the fillers, in that barrier enhancements were found to depend on the penetrant and did not clearly match morphological observations in terms of aspect ratio. The reason for this disagreement must be attributed to limitations of the models to account for factors such as polymer morphology and crystallinity alterations, irregular morphology and orientation of the filler platelets, chemical alterations in the matrix, and solubility of the penetrants in the filler.

The authors would like to acknowledge NanoBioMatters S.L., Paterna Spain for supplying clays and for financial support.

References

1. Petersen, K.; Nielsen, P. K.; Bertelsen, G.; Lawther, M.; Olsen, M. B.; Nilsson, N. H.; Mortensen, G. Trends Food Sci Technol 1999, 10, 52.
2. Haugaard, V. K.; Udsen, A. M.; Mortensen, G.; Hoegh, L.; Petersen, K.; Monahan, F. In Biobased Packaging Materials for the Food Industry—Status and Perspectives; Weber, C. J., Ed.; KVL Department of Dairy and Food Science: Copenhagen, 2001.
3. Arvanitoyannis, I.; Psomiadou, E.; Biliaderis, C. G.; Ogawa, H.; Kawasaki, H.; Nakayama, O. Starch/Stärke 1997, 49, 306.
4. Shuai, X.; He, Y.; Na, Y.; Inoue, Y. J Appl Polym Sci 2001, 80, 2600.
5. Reguera, J.; Lagaron, J. M.; Alonso, M.; Reboto, V.; Calvo, B.; Rodriguez-Cabello, J. C. Macromolecules 2003, 36, 8470.
6. Lagaron, J. M.; Catalá, R.; Gavara, R. Mater Sci Technol 2004, 20, 1.
7. Lagarón, J. M.; Cabedo, L.; Cava, D.; Feijoo, J. L.; Gavara, R.; Gimenez, E. Food Additives Contaminants 2005, 22, 994.
8. Cabedo, L.; Gimenez, E.; Lagaron, J. M.; Gavara, R.; Saura, J. J. Polymer 2004, 45, 5233.
9. Krishnamoorti, R.; Vaia, R. A.; Giannelis, E. P. Chem Mater 1996, 8, 1728.
10. Giannelis, E. P. Appl Organometal Chem 1998, 12, 675.
11. Vaia, R. A.; Giannelis, E. P. Macromolecules 1997, 30, 8000.
12. Dennis, H. R.; Hunter, D. L.; Chang, D.; Kim, S.; White, J. L.; Cho, J. W.; Paul, D. R. Polymer 2001, 42, 9513.
13. El-Hadi, A.; Schanabel, R.; Straube, E.; Müller, G.; Riemschneider, M. Macromol Mater Eng 2002, 287, 363.
14. Bucci, D. Z.; Tavares, L. B. B.; Sell, I. Polym Test 2005, 24, 564.
15. Koening, M. F.; Huang, S. J. Polymer 1995, 36, 1877.
16. Bastiolo, C.; Bellotti, V.; Del Tredici, G. F.; Lombi, R.; Montino, A.; Ponti, R. Int. Pat. Appl WO 92/19680 (1992).
17. Park, E. S.; Kim, M. N.; Yoon, J. S. J Polym Sci Part B: Polym Phys 2002, 40, 2561.
18. Tsuji, H.; Yamada, T. J Appl Polym Sci 2003, 87, 412.
19. Di, Y.; Iannac, S.; Sanguigno, L.; Nicolais, L. Macromol Symp 2005, 228, 115.
20. Feijoo, J.; Cabedo, L.; Gimenez, E.; Lagaron, J. M.; Saura, J. J Mater Sci 2005, 40, 1785.
21. Cabedo, L.; Feijoo, J. L.; Villanueva, M. P.; Lagaron, J. M.; Jiménez, E. Macromol Symp 2006, 233, 191.

22. Lim, S. T.; Hyun, Y. H.; Lee, C. H.; Choi, H. J. J Mater Sci Lett 2003, 22, 299.
23. Choi, W. M.; Kim, T. W.; Park, O. O.; Chang, Y. K.; Lee, J. W. J Appl Polym Sci 2003, 90, 525.
24. Hiltner, A.; Liu, R. Y. F.; Hu, Y. S.; Baer, E. J Polym Sci Part B: Polym Phys 2005, 43, 1047.
25. Crank, J. The Mathematics of Diffusion, 2nd ed.; Oxford Science Publications: Oxford, 1975.
26. Lagaron, J. M.; Powell, A. K.; Bonner, J. G. Polym Test 2001, 20, 569.
27. Cava, D.; Catala, R.; Gavara, R.; Lagaron, J. M. Polym Test 2005, 24, 483.
28. Barham, P. J.; Keller, A.; Otun, E. L.; Holmes, P. A. J Mater Sci 1984, 19, 2781.
29. Crescezi, V.; Mazini, G.; Calzolari, G.; Borri, C. Eur Polym Mater 1972, 8, 449.
30. Bershtein, V. A.; Egorov, V. M. Differential Scanning Calorimetry of Polymers; Ellis Horwood: New York, 1994.
31. Nielsen, L. E. J Macromol Sci (Chem) A 1967, 1, 929.
32. Fredrickson, G. H.; Bicerano, J. J Chem Phys 1999, 110, 2181.
33. Krook, M.; Morgan, G.; Hedenqvist, M. S. Polym Eng Sci 2005, 45, 136.
34. Hopfenberg, H. B.; Paul, D. R. In Polymer Blends; Paul, D. R.; Newman, S., Eds.; Academic Press: New York, 1978.
35. Lagaron, J. M.; Giménez, E.; Altava, B.; Del-Valle, V.; Gavara, R. Macromol Symp 2003, 198, 473.
36. Takahashi, S.; Goldberg, H. A.; Feeney, C. A.; Karim, D. P.; Farell, M.; O'Leary, K.; Paul, D. R. Polymer 2006, 47, 3083.
37. Merkel, T. C.; He, Z.; Pinnau, I.; Freeman, B. D.; Meakin, P.; Hill, A. J. Macromolecules 2003, 36, 6844.
38. Cava, D.; Gimenez, T.; Gavara, R.; Lagaron; J. M. J Plast Film Sheeting 2006, 22, 265.